Stringham, R. *Cavitation and Fusion - poster session*. in *Tenth International Conference on Cold Fusion*. 2003. Cambridge, MA: LENR-CANR.org. This paper was presented at the 10th International Conference on Cold Fusion. It may be different from the version published by World Scientific, Inc (2003) in the official Proceedings of the conference.

## CAVITATION AND FUSION ICCF10 POSTER

Roger Stringham

First Gate Energies, PO Box 1230, Kilauea, HI 96754 - firstgate@earthlink.net

#### **Abstract**

Natural cavitation phenomena in D<sub>2</sub>O using piezo devices, is now amplified initiating DD fusion events that produce heat and helium. We have adapted it for our use. The transient cavitation bubble, TCB, has been harnessed to produce high densities of deuterons, 10<sup>25</sup> to 25/cc. An electrically driven piezo device filled with D<sub>2</sub>O produces acoustic field generating TCBs that are, in the final collapse stage, micro accelerators. The result is the implanting of deuterons into a target foil producing <sup>4</sup>He originating from the Pd foil and T from the Ti foil. We are an emergent tangent technology to sonoluminescence, SL, technology, which we use to give us an environmental parameter probe into the bubble contents at the moment of its highest energy density. (Much of the SL studies center on the pulses of photons coupled to the irradiating acoustic field emanating from an oscillating single stable cavitation bubble, SSCB.)[1] The generation of these photons relates to conditions for the target implantation process. Recently we have been studying the effects of frequency on multi TCB SL conditions that produce fusion. These experiments and the analytical methods have concentrated on the mass spectroscopy of reactor gases, calorimetry of the reactor and power supply, and the scanning electron microscope photographs of target foils [2]. The results from many experiments are pieced together to reach a plausible path for the TCB that terminates with deuterons implanting into a target with the resulting fusion events. The use of SL for monitoring the bubble content's high energy densities allows for reactor parameter management for fusion events in the target foil. Studies of multi TCBs' SL at higher temperatures (300–450°K), external pressures (10<sup>6</sup>–10<sup>7.5</sup> dvnes/cm<sup>2</sup>) and frequencies (.02- 1.7 MHz) are proceeding in a search for better fusion environments. The results of these experiments will be presented.

#### Introduction

We have been performing experiments and developing the technology using TCBs for the controlled production of clean fusion energy with no associated long-range radiation. Recently our research has moved in the direction of small reactors at frequencies just in the megahertz range using SL as a tool indicating the presence of the bubble content dissociation during its adiabatic collapse process. It is of importance for the bubble contents in this transient environment to be dissociated as a high density, low energy plasma so that derterons can enter into fusion reactions. If a condition exits for a relatively large photon production from SL during the collapse process, then fusion events from the implanting jet will follow. Earlier work focused on .02 and .04 megahertz reactor systems successfully producing excess heat, <sup>4</sup>He and T without the use of SL to monitor and to assist in the adjustment of parameters to maximize fusion efficiency. Here we have reached the maximum energy density of the TCB contents. The parameters that are fundamental to this process are temperature, external pressure and acoustic input. The apparent increase of SL is due to the increase of effective bubble production with respect to fusion. It should be noted that as the frequency is increased from 0.02 to 1.7 MHz close to a 100-fold increase in frequency produces a substantial increase in SL pulses.

From the evidence we have collected from experiments and related SL papers a path to the produced fusion events is proposed and is only one of several path possibilities. The path starts in the TCB and its selected controlling parameters temperature, external pressure and acoustic input. These control the fusion environment. The bubble grows in the acoustic-field gaining  $D_2O$  mass from its surroundings, and then collapses in pseudo adiabatic accelerating mode forming a jet plasma from bubble contents; its last stage. The jet accelerates (launched from the TCB collapse) toward the target foil as a plasma which is further compressed via the z-pinch. The number of deuterons in the jet plasma is in the order of  $10^8$ . The lifetime of the implanting jet plasma is a few pico seconds. The high density implanted  $D^+$  in the target lattice transient trap [3] is the locale of DD fusion events producing an alpha and a heat pulse with no long-range radiation. The heat pulse reaching the target surface ejects as vapor some of the lattice leaving a vent site, a void, visible in SEM photos.

#### **Historical**

There have been some substantial successes in the past that will briefly be reviewed as they lead into the experiments using higher frequencies. These are the experimental results that show fusion events producing <sup>4</sup>He and T and FE SEM of vent site populations in target lattices. There are several reasons for using higher frequencies; one is the economics of the smaller devices and lower piezo voltages. And others are the induced frequencies in the target foil just over a MHz by the 0.02 and 0.04 piezo systems.

Helium production initiated from apparently low energy inputs has been measured in other related systems [4, 5, 6]. Our experiments using cavitation as the initiating source

at LANL's Tritium Facility in New Mexico produced helium. During these experiments Dale Tuggle and Tom Claytor assisted us. Brian Oliver performed measurements on the reactor gases at the DOE Laboratory at Rockwell Int., Canoga Park, CA. The gases over the  $D_2O$  in the reactor were collected, after the experiment, in stainless steel sampling volumes using a simple vacuum gas handling system that removed most of the gas. The results the mass spectrometry measurements are summarized in Table 1 and figure 1.

The analysis process was replicated for all runs; some produced helium, others did not. The removed gases from a blank run (non-helium producing run 4-1) analyzed for helium placed an upper limit for the <sup>4</sup>He in the argon supply tank. The <sup>4</sup>He was found to be less than 0.5 ppm. The 50 cc stainless steel sample cylinders were initially evacuated, then pressurized with the reactor gases via natural expansion and with 1/4 inch valves. The collected samples contained mostly argon with small amounts of deuterium from the recombination of dissociated D<sub>2</sub>O and the helium product gases. The D<sub>2</sub>O from Aldridge and the argon from Air Products were provided by LANL. These labeled sample volumes filled with reactor gases were delivered to the DOE laboratory facilities where Brian Oliver analyzed the sample volumes for <sup>3</sup>He and <sup>4</sup>He. See figure 1. The methodology of his analysis was to remove a small amount of gas (1 to 2%) for measurement and make three determinations of the gas content. The analysis performed by Brian Oliver involved passing the sampled gases through a hydrogen getter system at liquid nitrogen temperature removing any hydrogen species along with the dominant gases, Ar and D<sub>2</sub>O. The analysis focused on two mass numbers, 3 and 4 [7]. All measurements were made in triplicate and showed little scatter.

The gas measurements of generated helium removed from over the  $D_2O$  after the cavitation runs were analyzed as the collected gases in sample volumes 4-1, 4-2, 4-3 shown in Table - 1 and Fig. – 1. The gases present, besides the helium isotopes and argon were small amounts of  $D_2O$ , DOOD,  $H_2$ , HD and  $D_2$ , which were rarely measured [8] as they were usually removed. The reactor gases from the Pd target were collected in sample volume 4-3, which produced  $1.2 \times 10^{18}$  atoms of  $^4He$  (this amounted to 100 times the concentration found in air with over 500 ppm of  $^4He$ ) and if any  $^3He$  was produced, it was less than background. The reactor gases associated with the Ti target were collected in sample volume 4-2, which produced some  $^4He$  (5.9x10<sup>15</sup> atoms) and 3He. The measurement of  $^3He$  atoms spread over time represents the progressive decay of T atoms (To =  $6.8 \times 10^{13}$  atoms) in the sample volume 4-2. See figure 1 and Table 1. The calculated disintegration constant,  $\lambda$ , (the appearance of  $^3He$ ) was close to that of tritium; therefore, its identification as tritium.

The sample volume 4-1 was non-productive in helium isotopes and can be considered as a blank for both  $^4\text{He}$  and  $^3\text{He}$  measurements. This run being a normal run this number for the  $^4\text{He}$  background is more than fair. ( $^4\text{He}$  was measured at  $1.07x10^{15}$  atoms or 0.5 ppm which was used as a measure of  $^4\text{He}$  in the argon gas cylinder and  $^3\text{He}$  was at below background levels. Two channels for low energy nuclear events explain the results of these experiments with the first D + D  $\rightarrow$   $\alpha$  + heat and second D + D  $\rightarrow$  T + p + heat. No penetrating radiation was measured during the many hours of

cavitation or after. The tritium was in the form of DT or HT as T measurements of reactor  $D_2O$  were not significant. This is consistent with the fusion path we follow in this text.

One of the more informative tools is the use of field emission scanning electron microscope, FE SEM, photos of the surface of exposed target foils. Figure 2 presents several photos of a  $100\mu$  thick Pd foil target exposed to acoustically driven TCBs at 40 KHz in an Ar and  $D_2O$  environment and an analysis of the population distribution of the vent site diameter size. The upper photo is typical of the cavitation exposed target foil surface with a number of vent sites frozen into the palladium lattice. There is some magnification of surface topology and a count of sites and their size is shown in figure 2 as a graph of vent size population distribution.

Plasma impacts and vent sizes do not appear to be directly connected. This is determined from the energy distribution of the ejecta that is expelled from the vent site population. See graph. The energy of the jet plasma implant is 10<sup>-8</sup> ergs/implant and is expected to be confined, if there is an observable footprint, to an energy close to that of the dotted peak as illustrated in graph at 1500 nm. The impact of jet plasmas, which are spread over both sides of the target surface area, is shown in FE SEM photos. No obvious plasma jet implantation melt spots on the foil surface from the jet plasma contact have been observed, but we do see a wide size distribution of vent sites.

The high-density transient deuteron plasma implanted into the lattice created an environment for fusion events. These events were graphically revealed in FE SEM (field emission scanning electron microscope) photos of the exposed target foils. The discovery of the vent population with a size distribution range from 25 to 5000 nanometers in diameter fits a typical statistical distribution [2]. The top photo of the exposed Pd target foil shows the common small vent sites along with the population distribution with regard to size. A 1  $\mu$  sq. portion of the cavitation exposed surface shows more detail. The bottom of the figure shows a rarer larger vent site. When the environment for the fusion events is present, the foil records the ejecta sites as shown in FE SEM photos. A timeline represented in a step-by-step progression of the TCB into a plasma jet and its target implantation with the resulting fusion is shown in figure 10, finally culminates in the creation of a vent site in the target foil.

The heat pulse, generated by nuclear events deep in the target foil, travels to and erupts from the surface as ejected vaporous metal with the resulting formation of vents in the target foil. These vent sites are found covering the foil's exposed surface in FE SEM photos. One sq. µm, with a blowup located at the top right of the target foil surface indicates the random population density of the smaller vent site sizes. This photo shows, as other photos do, a numerical maximum for the size of sites between 75-100 nm with ejecta energy of about 20 Mev [2]. This value is close to the energy of one DD fusion event. Our report in the ICCF-8 Proceedings shows the distribution of the vent site population and the expected population of jet plasma implants generated from the TCB. The associated energy expected from an implant does not fit that of the ejecta site population found in the foil target. The ejecta site does not contain or show the

implant energy, but only the ejecta sites of DD fusion events [9]. The vent sites do not correlate with the implant process. The jet plasma implants are similar in energy originating from proto bubbles of a similar size, a natural sorting process. Therefore, an implant vent size should lie in the range of 1500 nm in diameter, 10<sup>-8</sup> Joules, twenty times the 75 nano-meters vent size maximum. An implant population distribution was not observed on the Pd target foil [2]. The lower photo is of a large event 5000 nm in diameter and a much less common event than the 75 nm diameter events, which were pointed out in the vent site population distribution. Frame 1 shows the vent site originating in a crater with several other large sites and is outlined in black. Frame 2 shows that outlined portion of the site and vent after its ejecta release. Frame 3 shows the interior of the vent and the structure at the bottom consisting of a jagged hole (hedgehog in configuration) less than a  $\mu$  in diameter. The energy to produce this big site would be a million times 75-100 nm ejection events. In conversation in 1996 with Yon Kucherov he pointed out, that from his knowledge, nuclear events in metal foils would produce such a hedgehog structure [10].

When a fusion event occurs, it usually takes place deep in the foil just after implantation generating in the trap an energy pulse that follows a channel of heat production rather than a gamma or some other energy dispersing mode. The heat pulse travels to and erupts from the surface as ejected vaporous metal with the resulting formation of vents in the target foil. These vent sites are easily found in FE SEM photos covering the foil's exposed surface.

### **Experimental**

The general form of the high frequency (1.7 MHz) multi-TCB collapse is shown in figure 1 with information incorporated from our work [11] and others [12-23] assuming the ideal symmetrical adiabatic collapse process. In the TCB multi bubble acoustic systems the collapse is neither symmetrical nor adiabatic so the figure is an over simplification of the collapse process [15]. In figure 1 there are three graphs showing the bubble and its collapse. It progresses from the initial bubble in the acoustic field to the bubble in its final stage - the jet and plasma formation - before implantation. The figure shows pressures and temperatures of the bubble contents as the diameter, R, is imploding at a velocity of Mach 4 (the inward velocity of the bubble surface)[17]. The lower graph shows the result of the SL generated photons from the transient cavitation bubble, TCB, implosive collapse passing through a grating that separates the SL energies into its characteristic distribution. The presence of sonoluminescence, SL, at these higher frequencies makes the use of small reactors, which leads to experiments that are more economical in money and time. SL is an important tool since it indicates the state of dissociation of the bubble contents and the jet's high-density plasma contents.

The one cycle TCB initiation, growth, and collapse in the figure 3 show some details of the coupling between acoustic waves and the TCBs. The initial bubble diameter, Ri, is selected from a large array of bubble sizes that are related to the frequency and amplitude of the acoustic wave. This bubble grows isothermally, the green zone, gaining extra mass via the bubble interface of  $D_2O$  and in the process moves into the +

pressure zone of the acoustic wave reaching a maximum radius Ro. At this point the TCB moves quickly into a pseudo adiabatic collapse, the red zone. The collapse is an imploding acceleration creating an environment for the dissociation of the bubble's D2O contents into deuterons and is defined by Rf, the final bubble diameter, which is about .01 of Ro. At the end of the collapse process at Rf there are many changes occurring within the bubble contents. Some important changes are; the formation of a high density and low energy plasma, the opacity of the contents of the bubble with its high density of free electrons, transient organizational changes within the contents to produce a high density, and low energy bubble jet. The blue zone shows the last stage of the bubble collapse with the jet formation and the 100 picosecond SL pulse emission. During these transient processes a window opens letting SL photons escape from the last stage of the collapsing bubble into the D2O. A Hamamatsu 3 HC 125 03 PMT measures the SL. Experimentally, the three important parameters, external pressure, temperature, and acoustic intensity are coupled to yield the optimum conditions for TCB cavitation; it is hoped that SL will aid in the control of these parameters promoting controlled fusion events

There is a difficulty of knowing and maintaining the environment for promoting fusion events in TCB systems and it seems obvious now to use SL as the tool of choice for this purpose. SL is a window into the TCB contents at the critical moment when the bubble reaches its maximum density and the plasma jet is formed. At this moment a burst of photons is emitted that is synchronous with the acoustic wave input which is the SL pulse. To effectively monitor the bubble environment we have developed a window of observation for this purpose on a small 1.7 MHz reactor. Using SL and the PMT counting of emitted photon pulses for the adjustment of the environmental parameters in the reactor to keep the photon pulse count at a level that provides for best conditions for tracking the fusion environment keeps control of the system. A correlation between photon emission and excess heat production is the goal for this work. The small mass 1.7 MHz reactor system, referring to lightweight and small size, is run at steady-state temperatures so the heat removal process becomes important to its overall operation. See figure 7. This is also a condition that makes the calorimetry much easier.

The measurements and setup for SL emission from the 1.7 MHz reactor is shown in figures 4, 5, 6, & 7. The correlation of SL emission with the 1.7 MHz system was accomplished using a SoftScope (SDS) oscilloscope with a 5 giga-sample/sec. capability that monitored the SL pulse PMT emission and acoustic input. Included in the experimental setup is a counter to measure the TTL pulse rate. One can see in the oscilloscope captured pictures from the 1.67 MHz input to the piezo, which acoustically drove the  $D_2O$ . The pictures show several just out-of-phase acoustic amplitudes contributing to overall SL. See figure 5. This is seen as a 150 nanosecond phase spread of photon pulses caused by input piezo voltages that are not quite coherent. The TTL SL pulse of the 70-nm half width generated by the PMT must be compared with the SL pulse width from the TCB of less than 100 picoseconds. The PMT will produce one TTL pulse from thousands of photons in one TCB pulse. There can be several TTL pulses caused by the amplitude spread and coherence problem. The pulse count from the system is associated with the photon pulse and not the number of

photons in a pulse and is true for 40 kHz and 1.7 MHz systems. External pressure, temperature, and acoustic input can control the PMT signal. See figure 6.

The operation of 20 and 40 KHz reactors did not have the advantage of the SL measurement control. These lower frequency systems measured the <sup>4</sup>He and excess heat production as proof of the ability to create transient fusion events. The 1.7 MHz system must go through the same stages of bubble growth, adiabatic collapse and jet production, so assumptions have been made that the 1.7 MHz system will parallel the 20 and 40 KHz systems [18]. This fits the high intensity of SL observed in the 1.7 MHz systems we are studying. The TCB size is much reduced perhaps by an order of magnitude. There is a new generation of TCB associated with each cycle that leads to a time frame 1/50 of that of a 20 KHz system. See figure 10. The time period of one cycle is equal to that of just the adiabatic collapse portion of the 20 KHz system. The width of this TTL pulse is 70 nano seconds and the time between the acoustic cycles is 600 nanoseconds. So the flood of photons that are in phase and coupled with the acoustic input saturate the PMT and show only one or two TTL pulses for thousands of photons produced during that short period. The acoustic input signal is composed of several in-phase amplitudes that spread the photon emission over 150 nanoseconds. Therefore, we see several TTL pulses spread across that short time period. With the reduced volume, mass, and TCB contents the number of SL photons/bubble is reduced from 106 at the low frequencies to 103 at the high frequencies. However, at 1.7 MHz the SL photon pulse density at the bubble's final diameter, Rf, increases via PMT pulse measurements of the multi TCBs. The PMT pulses at 40 KHz naturally have fewer pulses (1/40) since they are coupled to the acoustic frequencies. At these high frequencies the initial bubble sizes naturally selected are much smaller, Ri, and go though the sequential stages of growth and collapse in an abbreviated fashion. See figure 1. The high frequency TCB's transient size characteristics are scaled down from the 20 KHz TCB growth and collapse stages. The small size of the 1.7 MHz bubble can follow the increased speed of the physical processes that the higher frequencies force on the system. The symmetry of these smaller bubbles is higher since the influence of surface tension increases. There are two big physical differences in the reactors between the low and the 1.7 MHz operating frequencies. (1) The reactor thickness in the direction perpendicular to the piezo transmitter is a fraction of the ratio of the 0.02 MHz reactor (piezo driven wavelength)/(reactor thickness) which is 70 mm/6 mm compared to the ratio 1 mm/6 mm for 1.7 MHz reactor. (2) As mentioned above, the PMT pulses coupled to the acoustics is 40 times more at 1.7 MHz.

Figure 4 shows two graphs of SL at 40 KHz and 1.67 MHz measured via a grating indicating the photon energy frequency spread and the ability to use SL as a tool in the jet plasmas produced by TCBs. We know the TCB SL from our recent work and others' work in this field [24] and we have a correlation using the same physical set up of producing similar SL results. Two graphs show similar frequency distributions at 0.040 and 1.7 MHz. The first shows the effect of temperature and pressure on the 0.04 MHz SL system. The second shows the SL frequency distribution at 25° C of the 1.7 MHz system. The third graph shows the difference between 0.04 and 1.7 MHz - red and green dots - SL from Rf and the increase in SL for the higher frequency.

Figure 5 shows some modified and schematic measurements of the input of 1.7 MHz to the reactor water producing a SL output that is measured by the PMT. The two top graphs are modified copies from the PC SoftScope, 5 giga samples /sec., pictures. The right photo triggered on scope channel 1, the 1.7 MHz piezo input, and scope channel 2 is synchronous with the acoustic input and shows the SL PMT–TTL output. The left photo triggered on channel 1 measures 1.7 MHz input to the piezo and channel 2 measures the SL PMT output. The schematic in the lower part of figure 5 shows the multiple 1.7 MHz voltage amplitudes with the SL PMT TTL pulse synchronous with the reactor piezo frequency. The TTL are represented as the green photon sensing pulses for the 100-picosecond SL pulses, the red bars are the SL 100 ps pulses. The right side of figure 5 shows the wave in the reactor filled with D2O and a target foil. The wavelength of the 1.7 MHz input in D<sub>2</sub>O is about 1 mm.

SL is used as a tool to look inside at the final moments of the TCB collapse and connects the photon production to dissociation of  $D_2O$  into deuterons. The SL functions as a tool that relates in a qualitative way the deuteron transient concentration. In figure 6 this tool emerges showing the coupling between SL and changing parameters during the TCB production.

The measurement of the relative SL from a sono-fusion reactor should be kept close to its maximum by adjusting acoustic power, temperature, and external Ar pressure. Figure 6 shows data that gives us that control of the sono-fusion environment using this methodology. There is a problem comparing the output of different piezo frequencies, as mentioned in figure 4 text, which amounts to one TTL pulse per cycle that includes thousands of photons produced by the TCB SL pulse. The result is counting the TTL SL pulses and not the TCB photons which is not a problem if it is understood.

In figure 6, with 1.7 MHz acoustic input, the top graph shows PMT SL pulse count vs. temperature with 2 acoustic inputs 5 and 16 watts; two cavitating liquids, light and heavy water; and two external pressure gases, air and argon. There were eight systems studied as the temperature was varied. The light green with air saturated light water at 1 atm. pressure and a 5-watt acoustic input shows a decrease in SL as the temperature is increased as did all the systems. The dark green with air saturated light water at 1 atm. pressure and a 16 watt acoustic input also shows a decrease in SL as the temperature is increased along with a large increase in SL output. This indicates that more bubbles are entering into the SL process. The light blue with Ar saturated light water at 1 atm. pressure and a 5 watt acoustic input is consistent and shows a decrease in SL as the temperature is increased but is more intense and close to that of the light water with the 16 watt acoustic input. This is explained by the nature of the cavitation process and the polytropic constant,  $\gamma$ , between air and argon (PV $^{\gamma}$  = c). The final stage of the bubble Rf is hotter. The dark blue with Ar saturated light water at 1 atm. pressure and a 16 watt acoustic input also shows a decrease in SL as the temperature is increased and a large increase in SL over the 5 watt system. This indicates that Ar saturated TCB systems improve from the use of Ar as the source of external pressure like stable single bubble systems [19]. The comparable D<sub>2</sub>O systems were represented

by two points for each of four systems studied with shaded red outline circles with the appropriate color code. The  $D_2O$  points were consistent with the  $H_2O$  systems. No real difference between  $H_2O$  and  $D_2O$  could be determined with these measurements [19] so we can use the information from the many SL  $H_2O$  studies to help with our control of the environment for sono-fusion [1].

The efficiency of the power supply that drives the acoustic piezos is shown in the lower graph of figure 6. The measurements were made in this small reactor containing 25 cc of water, a mass 10 times that of the reactor. The water was heated from ambient temperature at different power settings to a few degrees C for a measured time period to the final recorded temperature. The result of this measurement is the 40% efficiency of the power supply for the 1.7 MHz reactor.

Figure 7 shows the sono-fusion reactor for measuring the temperature, the excess heat, the reactor gas external pressure, the acoustic input, and the accompanying SL measurements. The figure of the reactor system is color coded to help understand how it is put together. A brief description of how the reactor works and its problems follows. The light box pictured above serves as both a SL measurement device and an excess heat generation measurement device. The Joule heater in the reactor containment serves to calibrate the acoustic input to the reactor by comparative measurements since Joule heater and piezo are located in nearly the same space. The temperature and Ar pressure surrounding and in the reactor is monitored, as is the acoustic input. This is accomplished in the darkness of the light box which has an in and out circulation of air to help the interior of the box's steady-state temperature. The configuration of the water in the reactor and reservoir allows for the Ar gas pressure to be distributed equally on both sides of the fragile piezo. The effect of higher pressures of Ar and acoustic inputs on both SL and excess heat can be measured at 1.7 MHz. The TC and power supplied to the piezo driver and the Joule heater have their respective wattmeters and produce the majority of collected data.

The 5x15 mm and 100 µ thick target foil is placed into the reactor. The reactor D<sub>2</sub>O capacity is small, 2 or 3 cc, compared to 50 cc for the older low frequency reactors. The actual reactor volume is less than 1 cc. After filling with D2O, the reactor is tested before enclosure in the sealed aluminum containment. The sealed ports for the TC, Joule heater, piezo power and Ar gas pressure system are tight and checked by monitoring the external argon pressure. One of the main concerns is the heat removal from the reactor and the control of steady-state temperatures in the reactor with the controlled airflow. The airflow fan controls the heat loss from the system. A quartz window allows for the monitoring of the SL via the PMT. The Joule heater allows for the heat loss characteristics for a known watt input into the reactor containment [2]. The calorimetry follows the heat loss characteristics for the reactor, heat-out equals heat-in balance, and any reactor heat not accounted for is counted as excess heat [24]. The calorimetry is measured when the system reaches steadystate temperature. When the reactor is turned off, the small amount of gas from over the D2O can be removed in a sampling volume for <sup>4</sup>He determination [7]. The RF is a problem and can interfere with the data collection. To resolve that problem the system has a duty-cycle (time on and time off) so the system is running part time. This also helps the reactor heat removal problem.

#### **Mechanisms and Timelines**

Figures – 4 & 5 show the transient configuration of the TCB as it forms the plasma jet – "The deuteron micro-accelerator". The velocity normal to the surface has been measured exceeding Mach 4 [17], collapsing or imploding towards the bubble center. There is a skin or interface where the bubble contents meet the surrounding D<sub>2</sub>O and where the surface tension increasingly pulls the bubble interface inward during the collapse while attempting to maintain its spherical shape. There is also an increasing acoustic pressure force and liquid D2O momentum directed to the bubble center that adds to the acceleration of the bubble collapse process. Near the final stage of the collapse the interface, a growing part of the jet, in an accelerating motion propels itself pulling the interface along with some of the bubble's coherent plasma contents, into and through the bubble to form a jet plasma. See figure 8. The velocity of this process is several times the velocity of the bubble interface collapse velocity. This is the birth of the plasma jet with a velocity of 30 km/s. The creation of the jet from the fast collapse phenomena consists of a dense coherent plasma of deuterons and electrons with a vacuum or possibly electron core as illustrated in figure 8. This is the deuteron micro accelerator. (1/2mv2=3/2kT) T=10,000°K

Some of the adiabatically collapsing bubbles reside on or near the target surface, where during the positive portion of the acoustic wave, they produce a jet [22,23], from the plasma contents of the collapsing bubbles, as a final statement. In the last stages of the bubble collapse the formation of jet ions (D<sup>+</sup>, O<sup>-</sup>, Ar<sup>+</sup>, and OD) and electrons, acting together as a plasma, have a velocity of several times the interface velocity of Mach 4. For the most part the particles are uni-directional. The velocity flow of the interface during the jet's creation produces a core vacuum at the center for the high-density plasma jet system. The compression heating of bubble contents near the center of the bubble may not be at the temperatures that exist near the interface since the high velocity of the interface and the transient times do not allow complete particle communication (the e-velocity at 10<sup>4</sup> °K about 10<sup>7</sup> cm/sec). The plasma jet probably has an electron sheath on the outside and inside of the jet as shown in the inset of figure 8 [25]. The figure shows the right side of the bubble with its interface without contents. Arrows indicate the direction and relative flow of bubble contents into the plasma jet. The color of the bubble contents on the left side indicates the relative temperature of the contents going from cool blue to hot red. The collapse phenomena rate may be too fast for temperature equilibrium within the bubble contents. growing plasma jet takes deuterons that are pumped into the jet by the collapsing bubble interface. Electrons form both an outer and inner sheath of the jet, and with velocities close to a million meters/sec magnetically pinch the jet contents to higher This dense flow of uni-directed electrons according to the Biot-Savart Law produce a magnetic pinch. See figure 9. This is the z-pinch that stabilizes the plasma containing jet during its short lifetime. There is no time for kinks to form in this jet system as in the Tokamak and Stellarator type devices [25,26] because the implantation

is over in less than a picosecond. The electrons of the sheath are not uniformly distributed through the cross-section of the jet and help in the containment of the jet. The jet has a finite length on the order of a 0.5µm in the 1.7 MHz system. The jet in reality has a tapered cross-section and probably an increasing electron density leading to a larger pinch at the pointed end in the growing and accelerating jet. A rough calculation leads to a current in the range of 30 amps and a pinch in the range of 60 Tesla.

A 1.7 MHz TCB in its final collapse mode the bubble plasma contents transfer to the plasma jet. There is an imbalance between the compression pinch pressure and the outward escaping pressure with the former being greater. The current, I, is defined by the number of e-/cc in the plasma jet and their velocity. Their low density of 1015 electrons/cc or deuterons/cc hampers the pinch effect in use in the very large and expensive hot fusion systems and needs a magnetic boost [25]. In the TCB system a transient plasma jet produced by the TCB is 13 orders of magnitude greater in density and avoids many other shortcomings of the hot plasma reactors. The millions of TCBs produced in sono-fusion systems have, when compared to other systems, advantages regarding cost, durability, flexibility and environmental impact.

Timelines are developed for the 1.7 MHz system to show a path from the TCB to a fusion event are shown in figures 10,11, and 12. Figure 10 for the TCB developing into the implanting jet plasma, figure 11 for the plasma jet's implantation, DD fusion, and lattice ejecta. Figure 11 is an event timeline for the fast process just after the plasma jet implantation. Figure 10 shows a log timeline and couplings for the TCB dynamics for transition into a high-density plasma jet (a deuteron accelerator).

The #2 yellow zone timeline, log time in  $\mu$  seconds to a picosecond, starts with time running towards 0 (the complete TCB collapse). The #2 yellow zone timeline coupled with the entire figure's five other categories shows the initial bubble formation in the #1 & #4 light and dark blue zones. The initial bubble 0.3  $\mu$ m diameter, Ri, and the bubble's size progression via the log of the bubble's diameter in m $\mu$  follow its isothermal growth and adiabatic collapse. The radius reaches its 3 $\mu$ m maximum diameter, Ro, before collapsing adiabatically accelerating to its last stage at .03  $\mu$ m diameter, Rf, which is at this point forming a jet plasma that terminates with the jet implantation. All this takes place in a fraction of an acoustic cycle.

The acoustic wave is represented as the amplitude versus its log of time in the violet zone #3 and is produced by the 1.7 MHz piezo. The acoustic wave never finishes its last cycle as time slows to almost 0 in the log scale. The TCB collapse occurs in the first positive half of the acoustic wave.

The density, the #5 orange zone, of this process is also coupled to the yellow log timeline. The density starts at some point in the negative pressure portion of the acoustic wave. Ri has a density of 1020/cc and continues to expand losing some of its initial density, but gaining mass from the bubble's interface. At Ro, maximum diameter and energy, the TCB has a density of  $10^{18}/cc$  molecules and atoms (D<sub>2</sub>O and Ar). At

this point the system has its maximum mass just before going into a pseudo adiabatic collapse that lasts for a hundred nanoseconds and at Rf has a density of  $10^{23}$ /cc. At the end of the collapse the pinched plasma jet with a density of  $10^{24}$ /cc particles is formed along with the SL emission.

The number of particles (atoms and molecules) follows the timeline, the #6 green zone, and increases as mass is gained from the expansion of Ri with a particle number of  $10^6$  to Ro with a particle number of  $10^8$ . Some mass is lost during its collapse process to Rf with a particle number of  $10^7$  particles (there is the energy of dissociation of  $D_2O$  that is supplied by the collapse process) [27]. The process continues as particles are lost when the jet is formed losing those that are not moving in the same direction as the jet, with perhaps a particle number of  $10^6$  remaining in the jet. Of these only  $10^5$  deuterons will be implanted into the target foil.

The timeline, yellow, is logarithmic starting with  $\mu$ -seconds, then becoming faster as the progression of events quickens to a picosecond at the time of the jet implantation. The process starts in the  $D_2O$  with proto bubbles of radius, Ri, that are residual from the previous acoustic cycle. The acoustic wave progresses through the liquid in its negative pressure phase. The bubble grows isothermally, gaining mass, which partially fills the vacuum created by the expanding bubble surface. As the momentum of  $D_2O$ , the liquid surrounding the bubble, expands away from the bubble center, the  $D_2O$  vapors and aerosols from the bubble interface diffuse into the comparative vacuum of the bubble contents increasing its mass. This isothermal mass growth continues as the acoustic pressure wave crosses the node into its positive pressure phase. The bubble growth slows and then stops at its maximum diameter, Ro, containing maximum energy ending the isothermal growth process.

What follows is a rapid collapse process, perhaps not initially but pseudo adiabatic in nature, as the acoustic pressure continues to increase. Although the bubble has accumulated a small amount of D<sub>2</sub>O vapor, it is still essentially a vacuum, depending on acoustic input, frequency, temperature, and pressure. The increasing pressure reverses the direction of momentum and initiates the collapse of the partial vacuum bubble with the surrounding D<sub>2</sub>O mass. This and the external pressure, accelerates the bubble contents and its interface toward the bubble center. The velocities have been measured at around Mach 4 in the final stage [17]. This rapid event is less than a tenth of a µ second, at 1.67 MHz, where the driving force originates from an attempt to equilibrate the differential pressure between the external pressure over the D<sub>2</sub>O and the internal pressure of the partial vacuum of the bubble contents. In the adiabatic collapse process the bubble contents are heated by compression to the point of dissociation producing ions and free electrons and form a low energy high-density plasma, LEHD plasma jet. This LEHD plasma jet is responsible for the production of SL photons and plasma containing jets.

The LEHD plasma jet is produced at the end of the adiabatic bubble collapse process. The jet contents consist of electrons and ions, which are pinched via the magnetic field produced by the high velocity of plasma electrons. The pinch of the LEHD plasma jet,

during the transient time period, from the collapsed TCB to the target foil surface, compresses the jet contents. The jet is about 0.5 microns in length and 0.02 $\mu$  or less in diameter and is compressed as it extends from the bubble surface. At the time of implantation the LEHD plasma jet is at a maximum density. The D<sup>+</sup> and e-plasma density is compressed by the z pinch effect from the high velocity sheath electrons. These electrons, initially associated with the bubble interface, will form a containment sheath around the plasma jet. In the jet the density of the particles is increasing and the surface electrons move in a spiral but are still coupled to slower more massive deuterons keeping the plasma identity. It is the nature of the plasma, unlike particle beams where the forces between particles have little influence on each other, to flow as a cohesive body as long as the particle distance does not exceed the Debye length, which is not likely. See figure 9. The plasma of the bubble contents is pumped into the jet and accelerated and implanted into nearby target surfaces by this naturally occurring phenomena [22,23].

A log timeline, figure 11, shows that the events of implantation, fusion, and the ejecta processes all occur in the target foil noted by the green dots. The log time starts and is now with the implantation of the pinched jet contents and its high-density plasma deuterons. The log timeline, increasing towards infinity, starts with the pinched jet implantation of deuterons into the target lattice, the transient deuteron distribution and density, and is immediately followed by the fusion of deuterons and other nuclear phenomena such as transmutations. The mechanism for heat transport in the foil lattice originates from the transient high-density implant where fusion takes place. The timeline ends with vaporous metal ejected from the target. Heat dissipation from the foil as a result of DD fusion in the metal target lattice quickly propagates through the foil as a heat pulse to the  $D_2O$  and the reactor containment. These target lattice events are frozen after its cavitation exposure and can be examined by FE SEM photos at our leisure.

Going through this mechanism again with the addition of a few more details will answer some questions. The contents of the jet plasma have a high concentration of deuterons and electrons in one form or another and are directionally coherent. The high velocity of the LEHD plasma jet electrons produces a z pinch further increasing the jet density. There is a strong transient coulomb field produced, at the point where the implant traverses deep into the lattice, between the implanted and separated electrons and deuterons. The implantation of LEHD plasma jet electrons will appear as a Fermi gas in the immediate area in the lattice and are attracted to the just implanted deuterons in a target foil trap.

The event line shown in figure 12 as the implant of the LEHD, low energy high density, jet plasma into the lattice of the target foil is complete and focuses on the time just after the pinched jet plasma implant into the target lattice. At this instant there is an initial charge separation into a Fermi electron gas and the trapped deuterons. There is a window for the excess electron population that is accelerating to the D+ trap to produce D atoms. The presence of rapidly increasing D atoms that continue to combine at the interface of the trapped D+ produce a pressure wave in the D+ trap. In this environment

fusion event(s) occur in the traps perhaps induced by the compression shock wave. The interaction sequences are not fully understood. One or more DD fusion events will occur under the right conditions in these  $D^{\dagger}$  traps. The LEHD plasma jet implants high-density electrons and deuterons into the lattice of the target foil. Diffusion and the dispersing coulomb field between like charges places a limit on the deuteron fusion contact time  $\tau$ . On the other hand forces generated from the local abundance of electrons attracted towards the high density of the just implanted deuterons provide for a localized cooling and heating compression force. These counter coulomb forces stabilize the repulsion between deuterons through the creation of transient coherent condensed phase ion traps, liquid or solid phase. A similarity exists between this approach and a paper presented by Yeoung Kim and Alexander Zubarev [3]. We consider these transient ion traps of high density and temperature also having some of the properties of a Bose-Einstein Condensate (BEC).

#### **Discussion**

To elaborate further on this possibility very fast processes on the order of picoseconds occur involving electrons combining with the deuterons in exothermic reactions, producing deuterium atoms and some D2 removing heat in the process. A spherical distribution of deuterium atoms occupying a volume surrounding the 50 nm diameter deuteron trap rapidly grows further heating and cooling and compressing these coherent trapped deuterons. One can see that the rapid volume growth continues from the inside at the edge of the spherical trap of D+. These deuterium atoms will be forced into the adjacent Pd target lattice at very high transient loading results. The electron diffraction of the Pd lattice shows a 5% expansion of target Pd foil [11]. These lattice deformations that occur in target foils in both heavy and light water, particularly with Pd, have been captured on video, and reflect the above process. However, the gravimetric measurements performed by E. Storms indicate no deuterium in the lattice [28]. A momentum exchange between the trapped coherent deuterons and alpha formation is the channel for the dispersion of fusion energy. [29,3].

The environment, which exists for a picosecond, allows for the production of DD fusion events with a LEHD plasma jet density of  $10^{25}$  D<sup>+</sup>/cc, a diameter of 0.02 µm, a length of 0.5 µm, and a population of 106 deuterons or less. (These values are all approximate.) The  $\tau$  (fusion contact time) for these high-density deuteron fusion systems is short (several picoseconds). Comparing with other high-density systems like those of muon fusion and inertial confinement fusion, MF and ICF, to the D<sup>+</sup> traps in sono-fusion we see that sono-fusion has a similar environment (in the range of  $10^{25}$  D<sup>+</sup>/cc). The DD fusion occurs within a few picoseconds in spherical coherent ion traps located in the target lattice. These ion traps have diameters approaching those of a MF system of less than 50 nm. These densely populated D<sup>+</sup> traps have some of the characteristics of the BEC. The implanted deuterons in the ion traps are detained momentarily while encountering the electrons from the implanting jet plasma. The electrons race towards the high plus charge of the deuteron implant lattice trap. The coulomb barrier between lattice trapped D<sup>+</sup> is altered through a cancellation of repulsive charges between the population of interior D<sup>+</sup> in the trap. The deuteron trap rapidly loses its collection of D<sup>+</sup>

through electron and  $D^+$  exothermic combination,  $(D^+ + e^- \rightarrow D)$  and  $(2D \rightarrow D_2)$ . In the trap environment fusion occurs without long range radiation [11].

There is a period of a few picoseconds in the lattice traps where one or more heat producing fusion events can occur and in the process destroy the transient D<sup>+</sup> trap collection. There is an intense heat pulse generated from fusion events located in the lattice ion trap. There may be one or many fusion events that occur from one LEHD plasma jet implantation. This heat radiates out from its source in the lattice as a heat pulse, consisting of a gaseous lattice vapor, radiating to the surface boundary of the target foil. It bursts from the target surface as metallic vapor ejecta leaving a footprint in the form of lattice vent sites on the surface of the target foil [2]. The lattice vent sites from these events can be observed in FE SEM photos of metal targets. See figures 2 & 11. If the right conditions are present in the lattice more specifically in the high deuteron densities in the traps, the  $\tau$  can be extended into the picosecond range. In these photos is evidence, observed as vent sites on the surface of the foil, for fusion events, single or multiple. Frozen on the surface of the exposed target foils is the vent site population that is counted and plotted as size versus number. These vent sites are the result of the escape of the vaporous metal and gases including produced <sup>4</sup>He from the target foil. How much of the <sup>4</sup>He product is ejected existing in the gaseous ejecta or how much is transported to the target lattice and locked in place is a question. It seems from measurements that most <sup>4</sup>He is ejected. The smallest and most populous vent sites have a population correlation to an energy near 20 Mey per event.

The  $^4$ He and T products are ejected with the vaporous metal ejecta and measured by mass spectrometry [2]. These vents are easily detected in the cavitation exposed metal target foils via FE SEM photographs. When the LEHD plasma jet is compared to hot plasma DD fusion, which operates at the low density of  $10^{15}$  D $^+$ /cc, an extrapolation to the very high densities of the LEHD plasma jet creates a transient environment similar to ddµ, muon catalyzed fusion, and ICF, inertial containment fusion, experiments. The sono-fusion experiments performed produce fusion events, nuclear products and heat. The D $^+$  was converted to T, p,  $^4$ He,  $^3$ He, and heat with no long-range radiation detected.

How does the target implantation of the cavitation plasma jet fusion fit with other successful fusion systems? Figure 13 shows conditions, where fusion events are expected, in the white zone of the log plot of log DD separation versus log D/cc (density). A temperature scale is color coded at the top of the graph. A comparison is made between several known processes and the TCB cavitation jet implantation process, which are noted by symbol **O.** The ddµ muon catalyzed fusion, MF yellow triangle, [30] at 50K is compared to dde liquid, black triangle (normal deuterium liquid and no fusion expected) and the figure shows that fusion events are expected in the ddµ system. In the case of the hot fusion system, TF green triangle, of the Tokamak type, fusion is expected [25] as in inertial confinement fusion, ICF orange triangle, [31,32]. Some of the systems have very short confinement times that may not be long enough to produce fusion products. If a fusion event is to occur, it must have both the confinement time and density. The TCB jet implantation systems are on the border of this parameter. In the multi-bubble TCB jet implantation system there would be some

scatter in the distribution of the energy density in the bubble population numbers for each acoustic cycle. In a population of a million deuterons there may be a DD couple in a target lattice trap that has all the requirements to produce a fusion event. The red triangle represents a star and according to this graph would have fusion rates at very low temperatures. These fusion rates in stars are slowed down by high concentrations of other species that are not directly involved in the <sup>4</sup>He production by this path. Under some conditions points all show fusion in their history. Deuteron systems that exist in the gray area of the graph will support fusion and those in the white will not. The several plasma jet examples in the graph show that as the density increases in the plasma jet, the temperature for fusion can be reduced.

The examples shown in figure 11 vary from the interior of a star such as the sun to the liquid deuterium, dde, spanning several types of fusion environments. The TCB jet implant is formed when the acoustic input energy, in the proper environment, creates bubbles that collapse more violently than the SCB (stable cavitation bubble) and therefore, produce higher energy density in the bubble contents. The implanted jet plasma is a high-density low energy plasma. The high-density is acquired via the plasma jet, which is pinched by the magnetic forces that are produced through the high velocity plasma electrons. See figure 5. The TCB "Jet" is stabilized by this pinch effect. The high density low energy jet plasma contains the deuterons from the dissociated  $D_2O$  that are implanted into the target lattice that remain in place long enough, a few picoseconds, to produce transient fusion conditions before diffusion destroys the deuterons' fusion possibilities [23].

#### Rate of Fusion

When looking at the results of our experiments and applying them to our work with systems resonating at 1.7 MHz there are no real impediments. It appears that the scaling of time and TCB size still produces a good SL emission 1.7 MHz. This will allow us to directly control the jet plasma parameters monitoring the SL intensity. We think the rates for DD fusion with the 0.02 MHz systems, which were initiated by the pinched LEHDP jet contents implanting into a target foil, will also apply to a 1.7 MHz system. The fusion originating from a TCB followed by the jet implantation into the target foil is not new fusion physics. Hot fusion kinetics between deuterons at low densities, in the range of 10<sup>15</sup> D<sup>+</sup>/cc, is based on Gamow curves and the Lawson criterion [29]. However, at high densities the fusion path produced by cavitation and MF is different relying on the high densities and low DD separation. When TCBs produce transient deuterons in lattice traps with the exclusion of electrons extending the fusion contact time  $\tau$  allows for high probability for fusion events. Evidence of this was seen in numerous target foils of different composition. In this environment we observed DD fusion products including <sup>4</sup>He and T by mass spectrometry via a path that was initiated by TCB cavitation. Reducing the repulsion between deuterons through the creation of coherent condensed phase ion traps or electromagnetic interactions has been treated theoretically [27,3]. There has been some disparity between the theoretical and experimental approaches, but with a little stretch with regard to temperature. picosecond time frames, and local endothermic reactions, these theories become more

attractive. The experiments using 0.02 and 0.04 MHz reactors are used to determine rates of fusion. In our target lattice the environment, which existed for a picosecond, allowed for the production of DD fusion events in these deuteron traps. The jet plasma had a density of  $10^{25}$  D<sup>+</sup>/cc, a radius of 0.1 µm, a depth of 1 µm, and a population density of 10<sup>9</sup> deuterons in the bubble contents. (These values are all approximate average.) The high velocity plasma implantation of high-density deuterons into the lattice of the target foil is the first step of the fusion process. After the jet implantation, the deuteron fusion events occur within the first few picoseconds or less in coherent D<sup>+</sup> ion traps. - See FE SEM photos in figure 6. The fusion events resulted in the generation of large heat pulses producing ejecta leaving behind vent sites in the target lattice and nuclear products, <sup>4</sup>He and T, and excess heat [2]. These vents were easily detected in the frozen exposed metal target foils via FE SEM photographs. When the TCB jet implantation density 1025 D+/cc was compared to hot plasma DD fusion, operating at a low density 10<sup>15</sup> D<sup>+</sup>/cc and muon DDµ fusion high densities, the TCB sono-fusion appears to be a comfortable in between fit. These TCB initiated fusion events produced nuclear products and heat but no long range radiation. The D<sup>+</sup> was converted to T, p, <sup>4</sup>He, <sup>3</sup>He via T, and heat [7,24,33].

For 1.7 MHz input there are perhaps 1000 implanting jets formed in each acoustic cycle. The rate depends on the density of the deuterons/cc, n, in the local traps that implant the target lattice. The deuterons are considered as transferred intact, although transient, into the lattice from the pinched jet plasma. There can be further compression and heating in the trap, see figure 2. Figure 9 shows the DD fusion rate for one jet implantation, in a one cc volume during a one second interval. This is accomplished by multiplying the rate constant by K, which gives the number of probable DD fusion events for a given n, D<sup>+</sup>/cc, for single implant event, Rj = K/2(n)  $^2\sigma v$  [2,34]. The fusion cross section,  $\sigma$ , is  $10^{-26}$  cm<sup>2</sup>. The rate us based on a velocity, v, of deuterons at  $10^6$  cm/sec, a jet volume, VJ, of  $10^{-19}$  cc, N deuterons  $10^{5}$  and an energy confinement time,  $\tau$ , of  $10^{-19}$ <sup>12</sup> seconds. The K for the one jet implant fusion rate is t  $\overrightarrow{VJ} = 10^{-31}$ . The figure shows the DD fusion rate for one jet plasma in the 1.7 MHz reactor depends on the density produced in the trap. For example the probable number of DD fusion events for n = 10<sup>25</sup> for one jet plasma implant is 0.1. It is speculated that the implanted trap deuterons existed in the target lattice as coherent ions in a transient state analogous to the BEC, Bose Einstein Condensate, for just a few picoseconds. We assume that the energy density of the jet is transferred through the implantation to the target lattice traps where deuteron fusion occurs.

## **Summary Results – Acknowledgments**

There is a period of a few picoseconds in the lattice traps where one or more heat producing fusion events can occur and in the process destroy the transient  $D^{+}$  trap collection. There is an intense heat pulse generated from fusion events located in the lattice ion trap. This heat radiates out from its source in the lattice as a heat pulse, consisting of a gaseous lattice vapor, radiating to the surface boundary of the target foil. It bursts from the target surface as metallic vapor ejecta leaving a footprint in the form of lattice vent sites on the surface of the target foil [2]. The lattice vent sites from these

events can be observed in FE SEM photos of metal targets. If the right conditions are present in the lattice more specifically in the high deuteron densities in the traps, the  $\tau$  can be extended into the picosecond range. Fusion events, single or multiple can take place in the deuteron traps. The smallest and most populous vent sites have a population correlation to a minimum energy near 20 Mev. The  $^4\text{He}$  and T products are ejected with the vaporous metal ejecta and are freed for measurement by mass spectrometry [33]. These vents are easily detected in the cavitation exposed metal target foils via FE SEM photographs. The LEHD plasma jet is not compared to hot plasma DD fusion, which operates at the low density of  $10^{15}$  D $^+$ /cc, but a comparison exists between transient sono-fusion and MF catalyzed fusion along with ICF fusion experiments. The sono-fusion experiments performed produce fusion events, nuclear products and heat. The D $^+$  was converted to helium and heat with no long-range radiation detected

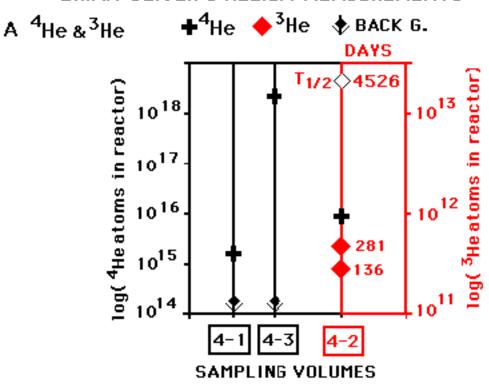
We had help over the years from F. Tanzella and M. McKubre of SRI, D. Tuggle and T. Claytor of LANL, D. Raymond, T. Passell, R. George, T Benson, J. P. Biberian, M. Srinivasan, E. Storms, S. Chubb, K. Wallace, W. McCarthy, J. Chandler, J. Wallace, Gene Mallove, Ken Rauen, Jan Roos, Jed Rothwell, John Dash, Jane Wheeler, Brian Oliver, G. Chambers, D. Nagel and others.

## **Figures**

Cavitation Thickness Time Hr in μm							Measured Products		
Run	n Target Foil		t	Cavitation Environmer		× Below Background			
4-1 4-2 4-3		Ti Ti Pd	100 100 254	D₂O/Ar D₂O/Ar D₂O/Ar		<sup>4</sup> He <sup>4</sup> He <sup>4</sup> He	He <sup>3</sup> He <sup>3</sup> He <sup>3</sup>	<b>;—</b> т	
Run	Atoms <sup>4</sup> He Produced n			Temporal Atoms <sup>3</sup> He Produced	T> <sup>3</sup> He Time in days			<sup>4</sup> He/T <sub>o</sub> Ratio	
4-1				×BBG					
4-28	5.9x10 <sup>15</sup>		٠ (	(0.0)		0			
4-2b				3.2×10 <sup>11</sup>		136			
4-20			(	6.5x10 <sup>11</sup> 6.8x10 <sup>13</sup>		184		10 <sup>2</sup>	
4-2d 4-3	10		8	xBBG		00 			
×BB0	3 He <sup>4</sup> =	= 10 <sup>1</sup>	4 <sub>v</sub>	BBG <sup>3</sup> He = 1	010	)		-	

Table 1. The summary of Brain Oliver's mass spectrometry data.

## **BRIAN OLIVER'S HELIUM MEASUREMENTS**



## APPEARANCE OF <sup>3</sup>He IN SAMPLE VOLUME 4-2

## **B** Tritium

$$^{3}$$
He =  $T_{0}$  (1-e<sup>- $\lambda$ t</sup>)

 $T = T_{0}$  e<sup>- $\lambda$ t</sup>
 $t_{1/2}$  for  $T = 12.4$  YR

 $T_{0} = 1.2X10^{13}$  ATOMS

TRITIUM  $\lambda = 1.89x10^{-9}$ /sec.

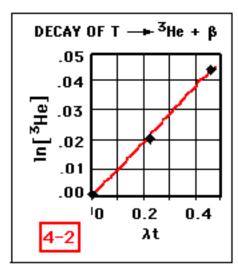


Figure 1. The results of the He measurements performed by Brian Oliver. Direct measurement of <sup>4</sup>He and the indirect measurement of T by way of temporal measurements of 3He.

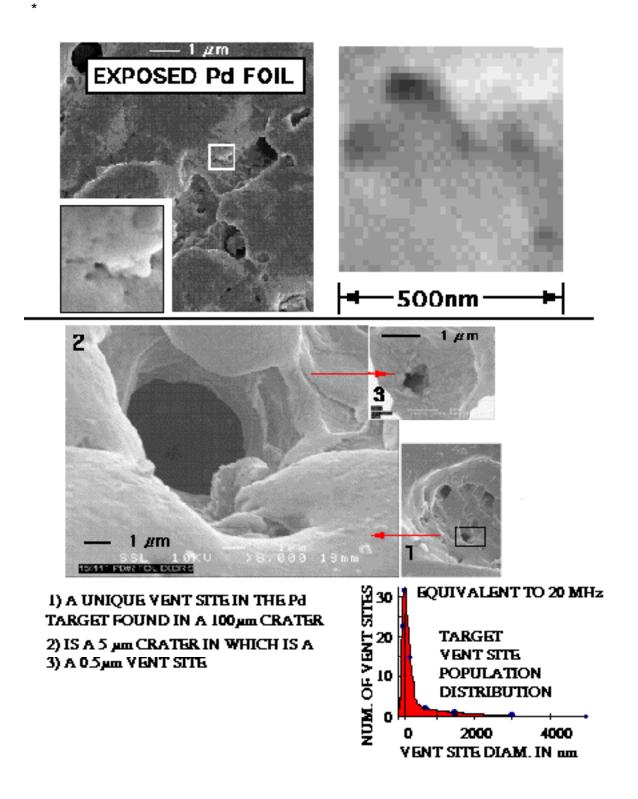


Figure 2. The FE SEM photos of a 100  $\mu m$  Pd target foil and the distribution of the vent site population.

## HIGH ENERGY TRANSIENT CAVITATION BUBBLE ONE ACOUSTIC CYCLE ISOTHERMAL GROWTH ADIABATIC COLLAPSE DENSITY INCREASE COLLAPSE FINAL STAGES R ACOUSTIC WAVE+ **IMPLANTATION** RADIUS DESTRUCTION 1.0 TIME NANO SEC. Ri SONOLUMINESCENCE µ SEC. D.3 TIME SONOLUMINESCENCE 15 сс Ң,0 @ 1.67 МНг 25% & 1 ATM. AIR RELATIVE NUM. 151 SL PULSES 10 5 500 600 400 700 PHOTON FREQUENCY IN nm

Figure 3. The 1.7 MHz TCB growth and collapse in one acoustic cycle and the SL energy distribution in water.

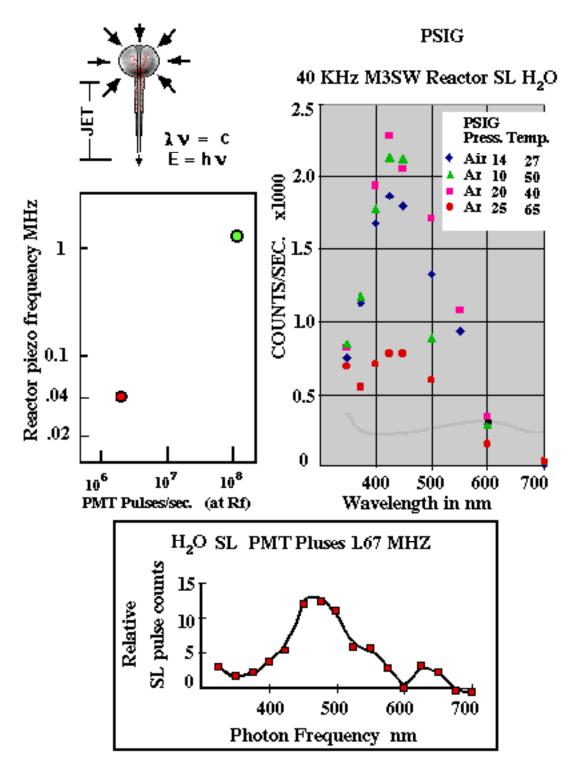


Figure 4. A comparison between the 0.4 and 1.7 MHz SL energies and a comparison of the photon pulses. SL provides a tool for the management of the environmental parameters so the fusion events can be maximized.

## SONOLUMINESCENSE @ 1.67 MHz (MULTI TCB)

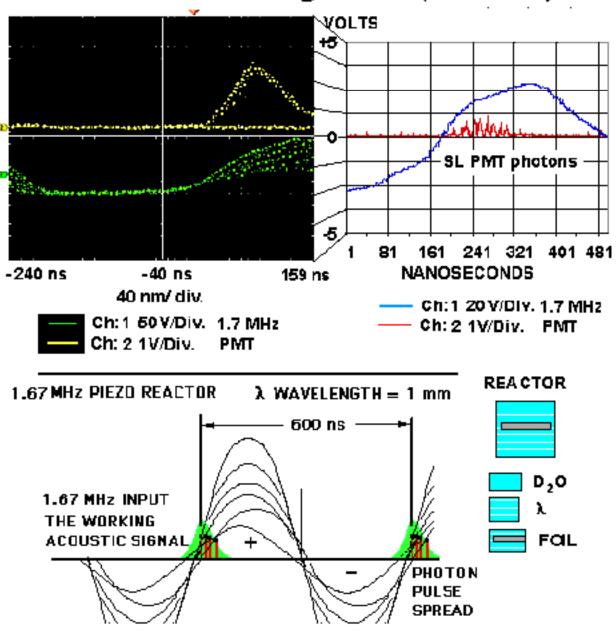


Figure 5. The oscilloscope output of the piezo input and the PMT TTL pulse with a schematic of their correlation.

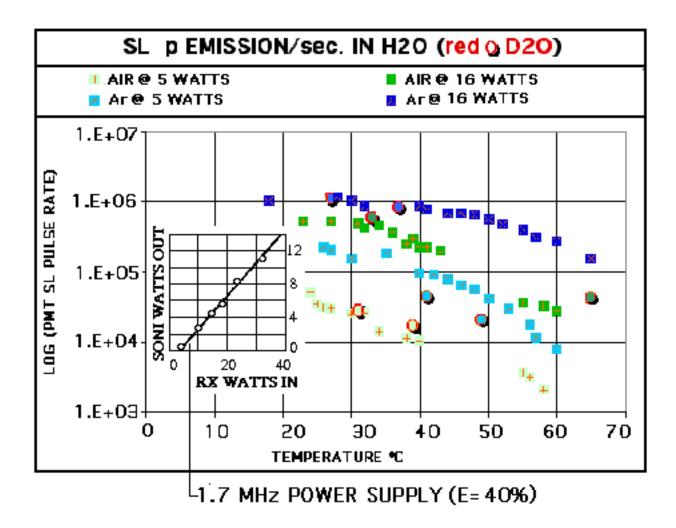


Figure 6. Data collected from the reactor regarding SL output in light and heavy water. The graph inset shows the efficiency of the reactor power supply with regard to acoustic input.

## SL 1.67 MHz Rx (photon counter)

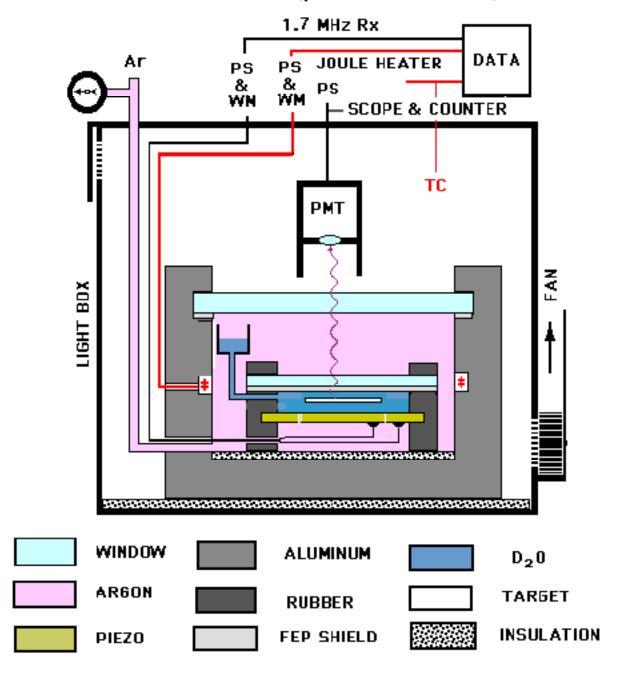


Figure 7. The 1.7 MHz reactor for producing excess heat using SL as the management tool to maximize the phenomena.

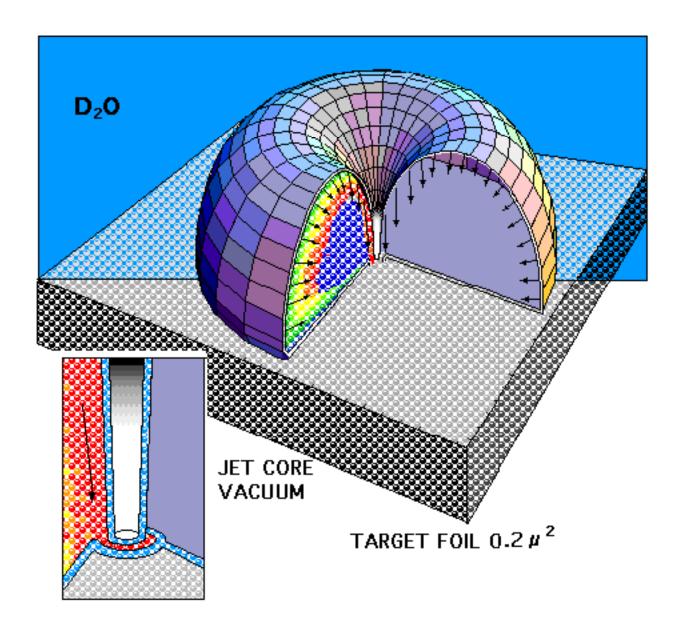
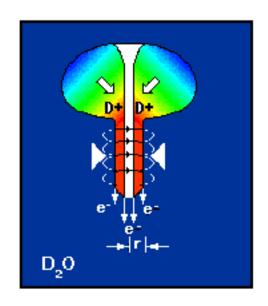


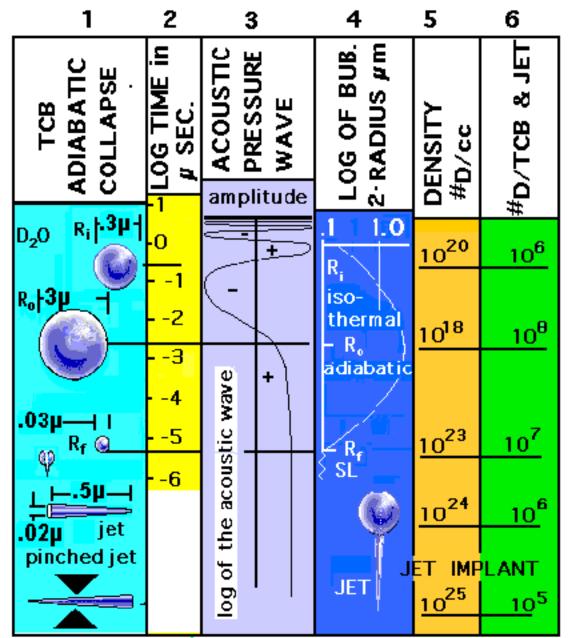
Figure 8. The final stage of the TCB collapse and its metamorphosis into a jet plasma accelerator for deuterons.

# Fast moving electrons in the jet produce a magnetic pinch that exceeds the escape pressure of the accelerating jet plasma.



$$v_e = 2\pi 10^5 \text{m/s}$$
 $r = 10^{-8} \text{m}$ 
 $n = e - / \text{jet } @ 10^7$ 
 $N = e - / \text{m}^3 = 10^{28}$ 
 $\mu = 4\pi 10^{-7} \text{Tm/A}$ 
 $V_{\text{int}} = 10^{-19} \text{m}^3$ 

Figure 9. The jet pinch effect that further compresses the jet plasma.



FOR 1.7 MHz SYSTEM -- INCEREASING INITIAL TEMP. & PRESS. INCREASES THE D<sup>+</sup>. A TEMP. OF 400 °K AND PRESS OF 10 ATM. AT WILL INCREAS. THE ENERGY DENSITY 10 TIMES.

Figure 10. The 1.7 MHz log timeline for the TCB collapse that shows its coupling to the other parameters.

## PLASMA JET IMPLANT, FUSION & EJECTA

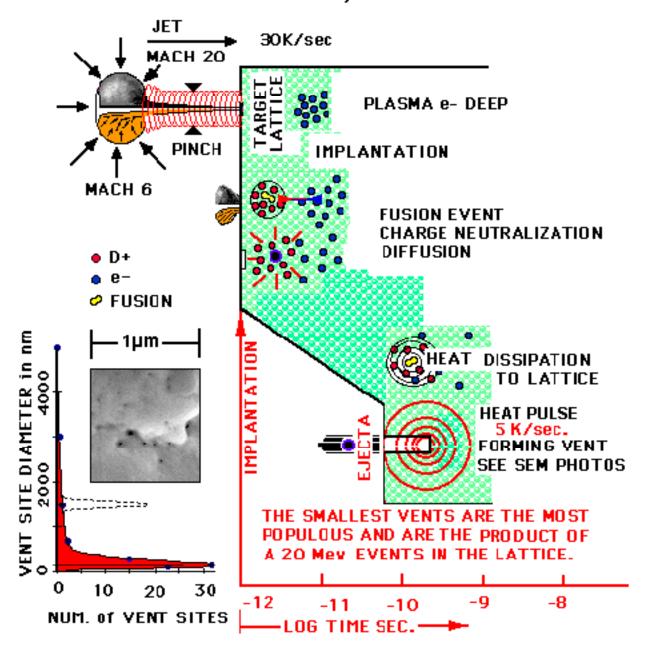


Figure 11. The log time line for the jet plasma implantation, fusion, heat pulse and ejecta that includes the <sup>4</sup>He.

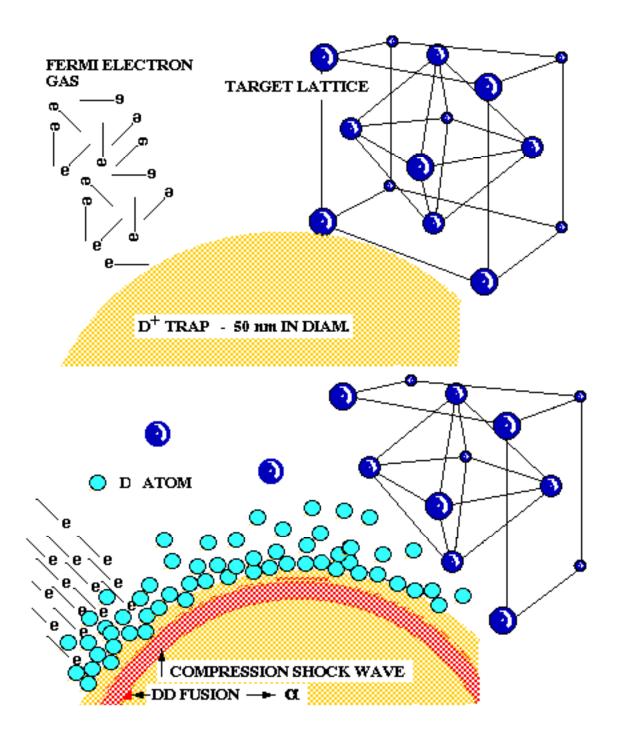


Figure 12 shows the event-line, transient, as events are occurring in the same time frame. The effect of D growth inward compressing remaining trapped  $D^+$  and at the same time diffusing away.

#### DENSITY & FUSION

- ♦ SONO-FUSION
- ➡ LIQUID DEUTERIUM
- ▼ INERTIAL CONFINMENT FUSION
- ▼ D·D MUON FUSION (AMBIENT TEMP.)
- STAR
- ▼ D·D HOT FUSION (LOW DENSITY HIGH TEMP.)

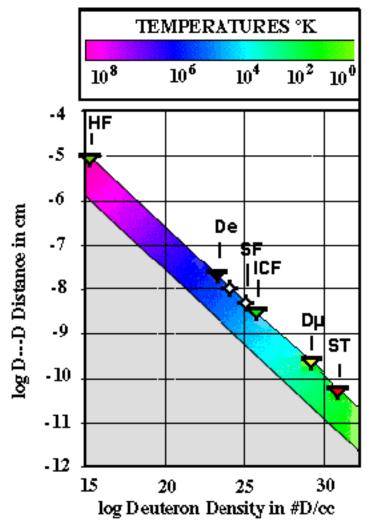


Figure 13. Various fusion systems and their respective separation and densities along with their relative temperatures.

## ONE IMPLANT FUSION RATE

 $R_{DD} = Kx0.5n^2\sigma v$  DD events/implant  $K = \tau(\text{jet Volume}) = 10^{-31} \text{ sec. cc}$ 

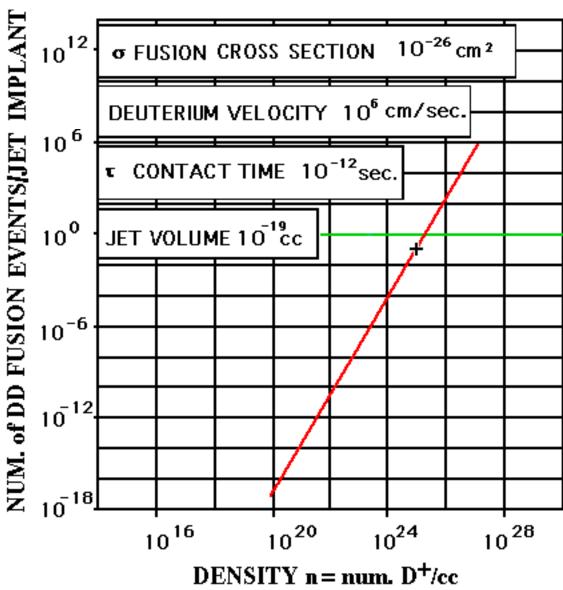


Figure 14. The rate of fusion using a 1.7 MHz reactor for one jet implant into a target foil. An example of a jet plasma implant at a density of  $10^{25}$  has the probability of producing 0.1 fusion events. This is a practical rate since billions of implants occur each second.

#### References

- [1] M. P. Brenner, Sascha Hilgenfeldt, and D. Lohse, Single-bubble sonoluminescence, Rev. of Mod. Phy., 74, 425- 484, (2002)
- [2] R. S. Stringham, Proceedings of ICCF-8, , 299–304 (2000)
- [3] Y. Kim and A. L. Zubarev, Proceedings of ICCF-8, 375-384 (2000)
- [4] M. H. Miles, B. F. Bush, Proceedings of ICCF-4, 156-159 (1994)
- [5] A. DeNinno, A. Frattolillo, A Rizzo, F. Scaramuzzi, and C. Alessandrini, Proceedings of ICCF-8, 29, (2002)
- [6] M. McKubre, F. Tanzella, P. Tripodi, D. Di Gioacchino, V. Volante, Proceedings of ICCF-8, 23 27, (2000)
- [7] Brian Oliver of DOE performed the helium three & four analysis measurements. His methodology involved removing any hydrogen species before each analysis (1994 5).
- [8] R. Stringham, ICCF-7 Proceedings, 361-365 (1998)
- [9] R. Stringham, Amer. Phys. Soc,. Seattle WA. Meeting, Mar. 11 15 (2001)
- [10] Yon Kucherov. During a conversation he, Yon Kucherov, pointed out in 1996, that from his knowledge, nuclear events in metal foils would produce such a hedgehog void in the lattice structure.
- [11] R. Stringham; Proceedings of the IEEE Ultras. Intern. Symp., Sendai, Japan, vol. 2; 1107 (Oct. 5-8 1998).
- [12] M. S. Plesset, R. B. Chapman, *J Fluid Mech.* 47, 283 (1971)
- [13] L. A. Crum, *J. Phys.*, Paris; 40; 131 (1979)
- [14] D. F. Gaitan and R. G. Holt, Acous. Soc. Of Am., 103, 3046, (1998)
- [15] R.K Gould, J. Acoust. Soc. Am., vol56, No. 6, 1740 (1974)
- [16] Hickling, R., Phys. Rev. Lett., Vol. 73, No. 21, 2853 [1994]
- [17] K. R. Weninger, P. G. Evans, and S. J. Putterman, Phys. E Rev., 61, 2 1063 (2000)
- [18] K. R. Weninger, C. G. Camara, and S. J. Putterman, Phys. E Rev., 63, 016310 (2000)
- [19] R. A. Hiller and S. J. Putterman, Phys. Rev. Lett., Vol 75, No.19, 3549 [1995]
- [20] Weninger, K. R., Barber, P. B., and Putterman, S. J., Phys. Rev. Lett., vol. 88, 3 [2002]
- [21] Toegel, R., Hilgenfeldt, S., and Lose, D., Phys. Rev. Lett., vol. 88, 3 [2002]
- [22] M.P. Felix, A. T. Ellis, Appl. Phys. Lett. 19, 484 (1971)
- [23] M. S. Plesset, R. B. Chapman, *J Fluid Mech.* 47, 283 (1971)
- [24] R. S. Stringham, Proceedings of ICCF-9, , 323 [ 2002]
- [25] Amasa S. Bishop, *Project Sherwood*; Addison-Wesley (1958)
- [26] The Jet Project and Prospects for Controlled Nuclear Fusion, Edited by R. S. Pease, R. J. Bickerton, and B. E. Keen; The London Royal Society; 1987
- [27] W. C. Moss, D. B. Clarke, J. W. White, and D. A. Young, Amer. Inst. Phys., 6, 9, 2979(1994)
- [28] È. Storms, During a visit to Storm's laboratory in New Mexico we measured an exposed Pd foil for deuterium loading and found none [1996].
- [29] S. R. Chubb and T. A. Chubb, Proceedings, 385-390, ICCF 9 57 [2002]
- [30] L. W. Alvarez, et al, Catalysis of Nuclear Reactions by  $\mu$  Mesons, *Phys. Rev.*; 105 1127 (1957)
- [31] G. B. Canavan, Prospects for Fusion Power, Ed. By S. O. Dean, Pergamon Press, 47 [1981]
- [32] H. Hora, *Plasmas at High Temperatures and Density*; Roder-Verlag Regensburg, Germany (2000)
- [33] Brian Oliver of DOE performed the helium three analysis measurements on sample 4-2 over a time period of 281 days. His methodology involved removing any hydrogen species before each analysis (1994 5)

[34]V..A. Kerkinski and Yu. A. Novikov, Theoretical Modeling of Cold Fusion, Russia, Novosibirsk, Novosibirsk State University (2002)